Large Deformation Effects in the Postbuckling Behavior of Composites with Thin Delaminations

G. A. Kardomateas*
General Motors Research Laboratories, Warren, Michigan

The postbuckling deformation of composites with thin delaminations is modeled through a procedure that is based on large deflections of the delaminated layer. The results on the stiffness and strain energy are compared with an approximate model that does not include those effects (thin film model). The influence of large deflections on the energy release rate that characterizes delamination growth is also studied. These effects are found to be significant, leading to a less stiff and more growth-resistant system than the thin film approximation. Furthermore, the end fixity conditions are found to play an important role in the postbuckling behavior. Finally, results of experiments that were performed on the postbuckling characteristics of kevlar/epoxy specimens with thin delaminations are discussed.

Nomenclature

D_i = bending stiffnesses
E = Young's modulus in the axial direction, Eq. (1)
E_u = second elliptic integral, end value
F_u = first elliptic integral, end value
G = energy release rate
H = thickness of the delamination
k = $\sin(\alpha/2)$
k_i = $\sqrt{P_{i,0}/D_i}$
L = length of the beam/plate
ℓ = delamination length
M_i = bending moments
P_i = axial forces
T = thickness of the beam/plate
U_i = strain energy
α = distortion parameter
δ = total shortening (axial displacement)
θ = angle at the section where delamination starts
ν_{13}, ν_{31} = Poisson's ratios
Φ = amplitude

Subscripts

u = upper part
l = lower part
b = base plate
1 = in-plane longitudinal direction
2 = normal (out-of-plane) direction
3 = in-plane transverse direction

Introduction

DELAMINATIONS occurring due to initial manufacturing imperfections or in-service loads can significantly affect the strength and stiffness of laminated composite components. These in turn can influence the performance characteristics, such as the energy absorption capacity of a composite beam system.[1]

Much work has been done on the subject recently (e.g., see Refs. 1-3). However, although the buckling point can be fairly well determined, the postbuckling behavior that ultimately governs the performance characteristics of the composite structure is not well understood yet.

Depending on the relative thickness and length of the delaminated layer, the stability problem has been shown (e.g., see Ref. 1) to involve "local" buckling of the delaminated layer or combined local and global (also called "mixed") buckling, i.e., transverse deflections for both the delaminated layer and the base plate. The local mode has also been referred to as "thin film" delamination.[3] For the mixed mode, an analytical solution for the initial postbuckling deflections was presented by Kardomateas and Schmueser.[1] The solution was based on a perturbation expansion as a power series of the slope at the section where the delamination starts. For the thin film (local) mode, a postbuckling solution was presented by Chai, Babcock, and Knauss.[3] This solution was based on the underlying assumption that no other part except the delaminated layer undergoes out-of-plane deflections.

In the following, the thin film model (typical of long and thin delaminations) will be considered. Large deformation effects will be studied by using the large deflection (elastica) equations for the buckled layer. A correlation will also be made with test results on kevlar/epoxy unidirectional specimens.

Analysis

Thin film (or local) delamination buckling occurs when the instability is initiated by the buckling of the delaminated layer. The delaminated through-the-width film of thickness H and length ℓ is symmetrically located in a beam-plate of thickness T and length L. A unit width is assumed. For simplicity reasons, the properties of the beam-plate are assumed homogeneous, linearly elastic, and, at most, orthotropic. Over the region of the delamination, the beam consists of two parts: the delaminated layer (upper part) and the part below the delamination (lower part, of thickness $T-H$). Outside the delamination interval we have the base laminate (or thickness T). Denote by D_i the bending stiffness of each part, $D_i = Et_i^3/[12(1-\nu_{13}\nu_{31})]$, where t_i is the thickness of the corresponding part and E the modulus of elasticity along the $x \equiv 1$ axis.

If instability is initiated by the buckling of the upper delaminated layer (at which case the end load on the upper part is the Euler buckling load), the critical compressive force is[1]

$$P_{loc} = (T/H)\frac{4\pi^2 EH^3}{12(1-\nu_{13}\nu_{31})\ell^2} \tag{1}$$

Received Oct. 8, 1987; revision received April 1, 1988.

*Senior Research Engineer, Engineering Mechanics Department; currently at the School of Aerospace Engineering, Georgia Institute of Technology, Atlanta, Georgia.

Thin Film Model

The theory was developed in Ref. 3, and its essential features are recapitulated here for the sake of completeness. It was based on the assumption that in the postbuckling stages only the delaminated layer undergoes flexural deflections and that both the lower part and base plate are in a state of pure compression (Fig. 1). Assume the postbuckled shape of the film to be

$$y_u = A(1 + \cos 2\pi x/\ell)/2 \tag{2}$$

In terms of the strain necessary to cause buckling of the film

$$\epsilon_{cr} = \frac{\pi^2}{3(1 - \nu_{13}\nu_{31})}\left(\frac{H}{\ell}\right)^2 \tag{3}$$

the strain in the base plate ϵ_0 was found from the condition of compatible shortening of the upper and lower parts (the underlying assumption was that, except for the delaminated layer, the rest of the plate is uniformly compressed with strain equal to ϵ_0):

$$\epsilon_0 = \frac{A^2\pi^2}{4\ell^2(1 - \nu_{13}\nu_{31})} + \epsilon_{cr} \tag{4}$$

Therefore, the load per unit width was given by

$$P = E\epsilon_0 T = \frac{D_u\pi^2 T}{\ell^2 H}\left[\frac{3A^2}{H^2} + 4\right] \tag{5}$$

The associated total axial displacement is that due to the flexural shortening of the film plus that due to the compression of the film and the base plate:

$$\delta = \int_{-\ell/2}^{\ell/2} \frac{1}{2}\left(\frac{dy}{dx}\right)^2 dx + \epsilon_{cr}\ell + \epsilon_0\ell_0 = \frac{A^2\pi^2}{4\ell} + \epsilon_{cr}\ell + \epsilon_0(L - \ell) \tag{6}$$

The total strain energy of the system consists of the membrane and bending energy of the film plus the energy of the compression of the lower part and the base plate:

$$U = \frac{Eh\ell}{2}[\epsilon_{cr}^2(1 - \nu_{13}\nu_{31}) + \nu_{13}\nu_{31}\epsilon_0^2] + \int_{-\ell/2}^{\ell/2} \frac{1}{2}D_u\left(\frac{d^2y}{dx^2}\right)^2 dx + \frac{E\epsilon_0^2\ell(T - H)}{2} + \frac{E\epsilon_0^2(L - \ell)T}{2} \tag{7a}$$

or

$$U = \frac{Eh\ell(1 - \nu_{13}\nu_{31})}{2}\left[2\epsilon_0\epsilon_{cr} - \epsilon_{cr}^2 + \frac{\nu_{13}\nu_{31}}{1 - \nu_{13}\nu_{31}}\epsilon_0^2\right] + \frac{E\epsilon_0^2(LT - \ell H)}{2} \tag{7b}$$

and the strain energy release rate G is[3]

$$G = \frac{\partial U}{\partial \ell} = \frac{Eh(1 - \nu_{13}\nu_{31})}{2}(\epsilon_0 - \epsilon_{cr})(\epsilon_0 + 3\epsilon_{cr}) \tag{8}$$

This model, however, does not satisfy the condition of equilibrium of forces and moments at the delamination interface. Indeed, the end moment (at $x = \pm\ell/2$) that arises from the postbuckled shape Eq. (2) for the delaminated film cannot be balanced, since the rest of the plate was assumed to undergo only pure compression. Furthermore, since it is known that the load in the postbuckling stage does not remain constant, the assumption that the membrane stress in the buckled laminate is the same as the buckling stress is only a first approximation.

From this discussion, the immediate conclusion is that in any event, flexural deflections are bound to occur in both the lower part and the base plate. Therefore, although instability can be initiated by the local buckling of the delaminated film, transverse deflections cannot be limited to the postbuckled shape of the film, and bending deformation necessarily will be induced to the rest of the plate.

Large Deflection Model

To represent the postbuckling behavior of the delaminated film, we use the exact theory of plane deformation of a prismatic bar that is restrained elastically at the ends by means of concentrated forces and moments. For the rest of the plate, since the flexural deflections are small, we use the technical beam theory of cylindrical bending. The conditions of geometrical continuity that will be enforced play an important role in the realization of the equilibrium states.

Let us first focus on the delaminated layer. In the buckled form, which is assumed to be symmetrical, denote by P_u and M_u the end forces and moments. In the following equations, the quantities at the right end are used (see Fig. 2). The moments and angles are assumed to be positive clockwise. Two variables play an important role: the end-amplitude for the compressed film Φ_u, and the distortion parameter, α, which is the angle of tangent rotation at the inflection point from the straight position. These are the generalized coordinates of deformation. In terms of those two quantities, relations between the end stress resultants P_u, M_u, as well as other coordinates of deformation such as end-slope θ and total flexural contraction e_u, can be found. The relations require the use of elliptic integrals. Denote

$$k = \sin(\alpha/2) \tag{9}$$

The first elliptic $F(\Phi,k)$ is defined by

$$F(\Phi,k) = \int_0^{\Phi} \frac{d\phi}{\sqrt{1 - k^2\sin^2\phi}} \tag{10a}$$

and the second elliptic integral by

$$E(\Phi,k) = \int_0^{\Phi} \sqrt{1 - k^2\sin^2\phi}\, d\phi \tag{10b}$$

The values of those integrals at the end $F(\Phi_u,k)$, $E(\Phi_u,k)$ are denoted by F_u, E_u. The following five relations define the characteristics of the postbuckled delaminated layer[5]:

Axial force:

$$P_u = 4D_uF_u^2/\ell^2 \tag{11a}$$

End moments:

$$M_u = 4(D_u/\ell)kF_u\cos\Phi_u \tag{11b}$$

End rotations:

$$\theta = 2\arcsin(k\sin\Phi_u) \tag{11c}$$

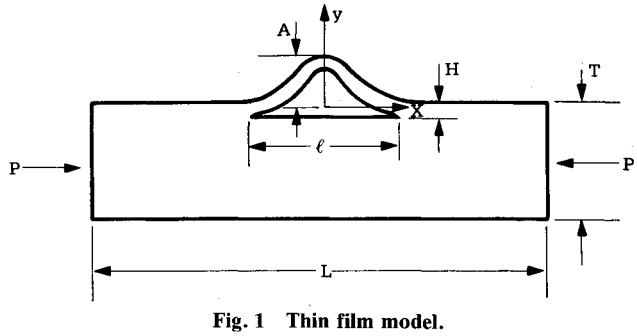

Fig. 1 Thin film model.

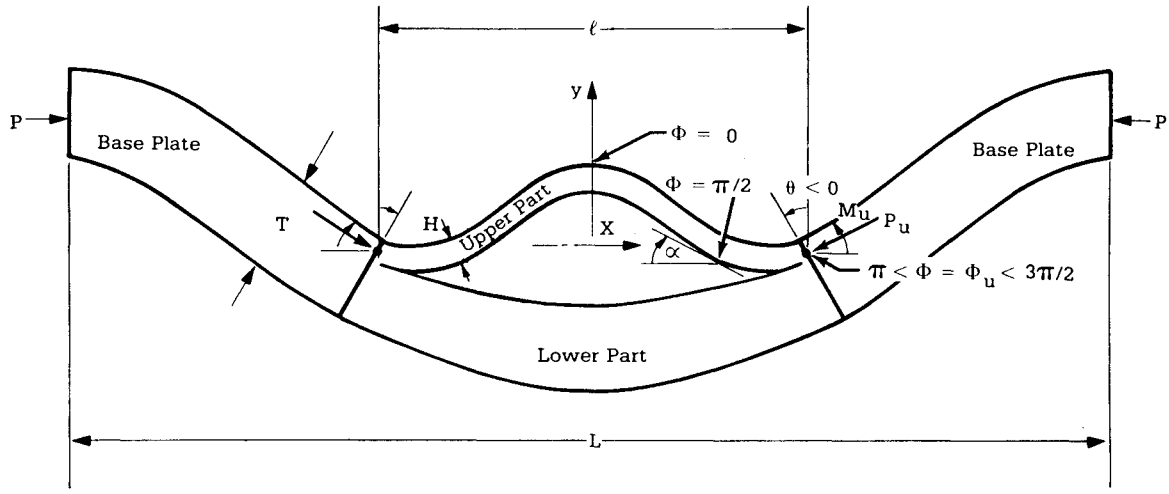

Fig. 2 Large displacement model illustrating the details for the geometry of the upper delaminated part at the postbuckling stages.

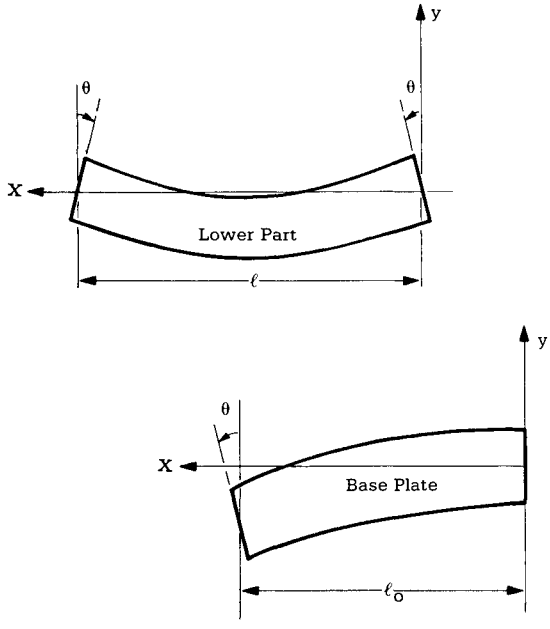

Fig. 3 Definition of the geometry for the lower part and the base plate.

Flexural contraction:

$$\lambda_u = e_u/\ell = 2[1 - (E_u/F_u)] \tag{11d}$$

Flexural elastic energy:

$$U_u = 8(D_u/\ell)F_u[E_u - F_u \cos^2(\alpha/2)] \tag{11e}$$

Furthermore, the deflection at the middle, normal to the central line of thrust (direction of axial forces P_u), Y_{um} is found from

$$Y_{um} = 2k\sqrt{D_u/P_u}(1 - \cos\Phi_u) \tag{12a}$$

It should be noted that each point x there corresponds a value of the variable Φ (amplitude for compressive members); the value at $x = \ell/2$ is Φ_u. Furthermore, at the inflection point, where the slope $\theta = \alpha$, the value is $\Phi = \pi/2$ and at the middle $x = 0$, where $\theta = 0$, $\Phi = 0$. With these remarks in mind, the deflections at all other points now are given from

$$y_u(x) = 2k\sqrt{D_u/P_u}\,[\cos\Phi(x) - \cos\Phi_u] \tag{12b}$$

where $\Phi(x)$ is found from the implicit relation

$$F[\Phi(x),k] = 2F_u x/\ell \tag{12c}$$

For the lower part and the base plate, since the induced bending is moderate, we use the technical theory of cylindrical bending under applied end moments and axial forces. We refer to the coordinate systems defined in Fig. 3. The differential equation to be satisfied for a beam under combined applied moments and compressive forces can be found in Ref. 6. For the lower part, the deflections satisfying the condition of end slope θ are given by

$$y_l = \left[\frac{\theta}{k_l \sin(k_l\ell/2)}\right]\left\{\cos\left[\left(\frac{k_l\ell}{2}\right) - k_l x\right] - \cos\left[\left(\frac{k_l\ell}{2}\right)\right]\right\} \tag{13a}$$

where

$$k_l^2 = P_l/D_l \tag{13b}$$

The end moment is expressed by

$$M_l = -D_l y_l''|_{x=0} = D_l k_l \theta \cot(k_l\ell/2) \tag{13c}$$

The flexural shortening is

$$e_l = \frac{1}{2}\int_0^\ell y_l'^2\,dx = \frac{\theta^2(\ell k_l - \sin k_l\ell)}{4k_l \sin^2(k_l\ell/2)} \tag{13d}$$

and the flexural energy is

$$U_l = \frac{D_l}{2}\int_0^\ell y_l'^2\,dx = \frac{D_l\theta^2 k_l(\ell k_l + \sin k_l\ell)}{4\sin^2(k_l\ell/2)} \tag{13e}$$

For the base plate (Fig. 3), the deflections satisfying the condition of end slope θ are given by

$$y_b = \theta\frac{(1 - \cos k_b x)}{k_b \sin k_b\ell_0} \tag{14a}$$

where

$$k_b^2 = P/D_b \tag{14b}$$

The end moment is given by

$$M_b = -D_b y_b''|_{x=\ell_0} = -D_b k_b \theta \cot k_b\ell_0 \tag{14c}$$

The flexural shortening for both parts of the base plate is

$$e_b = 2\int_0^{\ell_0} \frac{y_b'^2}{2}\,dx = \frac{\theta^2(2\ell_0 k_b - \sin 2k_b\ell_0)}{4k_b \sin^2 k_b\ell_0} \tag{14d}$$

and the flexural energy is

$$U_b = 2\int_0^{\ell_0} \frac{D_b y_b''^2}{2}\,dx = \frac{D_b\theta^2 k_b(2\ell_0 k_b + \sin 2k_b\ell_0)}{4\sin^2 k_b\ell_0} \tag{14e}$$

For the case of simply-supported ends, the deflections of the base plate are

$$y_b = \theta\frac{\sin k_b x}{k_b \cos k_b\ell_0} \tag{15a}$$

where k_b is given by Eq. (14b). In this case the end moment is expressed by

$$M_b = -D_b y_b''|_{x=\ell_0} = D_b k_b\theta \tan k_b\ell_0 \tag{15b}$$

and the flexural shortening for both parts of the base plate is

$$e_b = 2\int_0^{\ell_0} \frac{y_b'^2}{2}\,dx = \frac{\theta^2(2\ell_0 k_b + \sin 2k_b\ell_0)}{4k_b \cos^2 k_b\ell_0} \tag{15c}$$

The flexural energy is, in turn,

$$U_b = 2\int_0^{\ell_0} \frac{D_b y_b''^2}{2}\,dx = \frac{D_b\theta^2 k_b(2\ell_0 k_b - \sin 2k_b\ell_0)}{4\cos^2 k_b\ell_0} \tag{15d}$$

The following conditions of force and moment equilibrium at the interface section should be fulfilled:

$$P = P_u + P_\ell \tag{16a}$$

$$M_u + M_l - M_b = P_u(T-H)/2 - P_l H/2 \tag{16b}$$

Moreover, a condition of compatible shortening for the upper and lower parts reads

$$e_u + (1-\nu_{13}\nu_{31})\frac{P_u\ell}{EH} - e_l - (1-\nu_{13}\nu_{31})\frac{P_l\ell}{E(T-H)} = T|\theta| \tag{17}$$

The total shortening of the beam is

$$\delta = e_b + 2\frac{(1-\nu_{13}\nu_{31})P\ell_0}{ET} + e_u + \frac{(1-\nu_{13}\nu_{31})P_u\ell}{EH} - |\theta|(T-H) \tag{18}$$

where e_u, e_b are given by Eqs. (11d), (14d), or (15c).

The total strain energy of the system is that due to both bending and compression of the different parts

$$U_{tot} = U_u + \frac{P_u^2\ell}{2EH} + U_l + \frac{P_l^2\ell}{2E(T-H)} + U_b + \frac{P^2\ell_0}{ET} \tag{19}$$

where U_u, U_l, U_b are given by Eqs. (11e), (13e), (14e), or (15d).

Let us now consider delamination growth. It is assumed that whether further delamination occurs depends on the magnitude of the fracture energy, defined as the energy required to produce a unit of new delamination. To this extend, a Griffith-type fracture criterion is employed, and the postbuckling solution that has been obtained above can be used to calculate the energy-release rate as a function of applied axial displacement. This quantity is the differential of the total potential energy with respect to the delamination length. This method was used to calculate G in the thin film approximation. Alternatively, the path-independent J-integral concept (e.g., see Ref. 7) may be used to derive the energy release rate from the current stress and displacement distribution. This method was applied for a one-dimensional delamination[8] and resulted in an algebraic expression for the energy release rate in terms of the axial forces and bending moments acting across the various cross sections adjacent to the tip of the delamination. Since the end moments and forces are a direct output of the solution, the formula in Ref. 8 can be conveniently used in our formulation. The fact that large displacements are considered for the upper part does not affect the formula as long as the underlying assumptions are still valid, i.e., as long as we assume linearly elastic material, the bending stress to be linearly distributed through the thickness and the out-of-plane strain to be zero. In terms of the quantities

$$P^* = (D_l/T)k_l^2 H - 4(D_u/T)(F_u^2/\ell^2)(T-H) \tag{20a}$$

$$M^* = 4(D_u/\ell)kF_u\cos\Phi_u \tag{20b}$$

$$M^{**} = P^*T/2 - M^* \tag{20c}$$

the energy release rate per unit width is expressed as

$$G = \frac{6(1-\nu_{13}\nu_{31})}{E}\left\{\frac{P^{*2} + 12(M^*/H)^2}{H} + \frac{P^{*2} + 12[M^{**}/(T-H)]^2}{T-H}\right\} \tag{21}$$

Solution Procedure

For a given end rotation angle θ, we obtain the following system of equations in α (the tangent rotation at the inflection point on the delaminated film) and k_l (end load variable for the lower part), by substituting Eqs. (11), (13), and (14) or Eqs. (15) into (16) and (17):

$$4(D_u/\ell)F_u\cos\Phi_u\sin(\alpha/2) + D_l\theta k_l\cot(k_l\ell/2) + D_b\theta k_b\cot k_b\ell_0 - 2(D_u/\ell^2)(T-H)F_u^2 + (D_l/2)Hk_l^2 = 0 \tag{22}$$

$$2\ell\left(1-\frac{E_u}{F_u}\right) - \frac{\theta^2(\ell k_l - \sin k_l\ell)}{4k_l\sin^2(k_l\ell/2)} + 4(1-\nu_{13}\nu_{31}) \times \frac{D_u F_u^2}{E\ell H} - (1-\nu_{13}\nu_{31})\frac{D_l k_l^2\ell}{E(T-H)} - T|\theta| = 0 \tag{23}$$

where

$$\Phi_u = \arcsin[\sin(\theta/2)/\sin(\alpha/2)] \tag{24a}$$

$$F_u = \int_0^{\Phi_u} \frac{d\phi}{\sqrt{1-\sin^2(\alpha/2)\sin^2\phi}} \tag{24b}$$

$$E_u = \int_0^{\Phi_u} \sqrt{1-\sin^2(\alpha/2)\sin^2\phi}\,d\phi \tag{24c}$$

$$k_b = \sqrt{4(D_u/D_b)(F_u/\ell)^2 + (D_l/D_b)k_l^2} \tag{24d}$$

Thus, for a given end rotation angle θ the equilibrium state is found by numerically solving Eqs. (22) and (23). Notice that

the angle $\theta<0$ in Fig. 2. Moreover, in solving the system, the angle α is varying between θ and $\pi/2$, and the load P_l between zero and the buckling load for the lower part. (In fact it is found to be a small fraction of that buckling level.) Notice that the end amplitude Φ_u is $\pi \leq \Phi_u \leq 3\pi/2$. Thus, the equilibrium states are found by determining the values of α and k_l (or, equivalently, P_l) that satisfy the compatibility condition [Eq. (17)] and the equilibrium condition [Eq. (16)] at the delamination interface.

Results and Discussion

The postbuckling behavior predicted by the above analysis, which includes the effects of large deflections, is illustrated in the following. Consider a delaminated beam/plate with $L/T = 16$, delaminated layer thickness $H/T = 1/15$, and delamination length $\ell/L = 1/2$. For this case, the characteristic equation for the critical load (e.g., see Ref. 1) has no solution less than the local buckling load, i.e., buckling is initiated by the local buckling of the delaminated layer at a load P_{loc} given by Eq. (1). Figure 4a shows the load vs axial displacement curves. The Euler buckling load for the undelaminated composite with clamped-clamped ends is P_{glo}:

$$P_{\text{glo}} = \frac{4\pi^2 ET^3}{12(1-\nu_{13}\nu_{31})L^2} \tag{25}$$

The load values are normalized with respect to the Euler buckling load of the thin delaminated layer; C-C represents the case of clamped-clamped and S-S the case of simply supported ends. The thin film approximation is represented by the dashed curve. Notice that this approximation does not take into account the end fixity and thus cannot distinguish between the clamped-clamped and simply-supported cases. An immediate observation is that the thin film approximation would predict a stiffer postbuckled configuration. More important, however, is the leveling out of the $P-\delta$ curve, which represents a significant loss of stiffness for the system. The load level at which this leveling out occurs is largely affected by the end fixity.

At the point of local buckling P_{loc}, there is not any significant loss of the load carrying capacity of the whole system; however, this is not the case for the delaminated layer that essentially suffers a substantial loss of load carrying capacity. Figure 4b shows the corresponding to Fig. 4a curves for the load carried by the upper delaminated layer P_u. It is obvious that the applied load beyond the local buckling point is carried by the rest of the system.

Figure 5 shows the variation of the strain energy of the system with the axial displacement. Both the cases of clamped-clamped (C-C) and of simply-supported (S-S) ends are shown. Again, the end fixity plays a significant role in the stored energy. The thin film approximation predicts a larger amount of energy. It also gives a continuously much steeper curve. On the contrary, the large displacement analysis gives curves that eventually have an almost constant slope. Notice that the energy per unit applied displacement is larger for the clamped-clamped case.

Growth of the delamination can be studied by calculating the strain energy release rate. Figure 6 illustrates the variation of the energy release rate with applied axial displacement. Again, the end fixity influences the magnitude of G, the

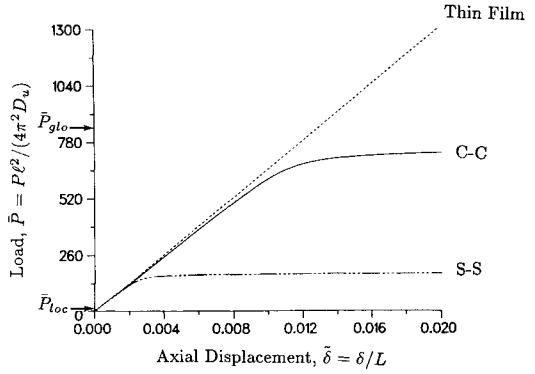

Fig. 4a Load vs displacement curves for a delaminated beam/plate with $L/T = 16$, $H/T = 1/15$, $l/L = 1/2$; P_{glo} is the Euler buckling load for the undelaminated composite and P_{loc} is the local buckling load. The load is normalized with respect to the Euler buckling load of the thin delaminated layer. C-C represents the case of clamped-clamped and S-S the case of simply supported ends. The dashed curve represents the thin film approximation.

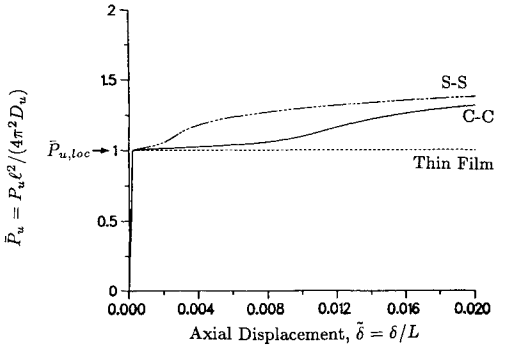

Fig. 4b Load carried by the upper delaminated layer vs displacement, corresponding to the curves of Fig. 4a. The load is normalized with respect to the Euler buckling load of the thin delaminated layer.

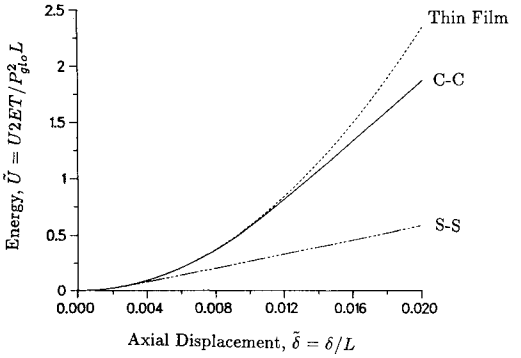

Fig. 5 Energy vs axial displacement curves for a delaminated beam/plate with $H/T = 1/15$, $l/L = 1/2$. Both the cases of clamped-clamped (C-C) and of simply supported (S-S) ends are shown. The dashed curve represents the thin film approximation.

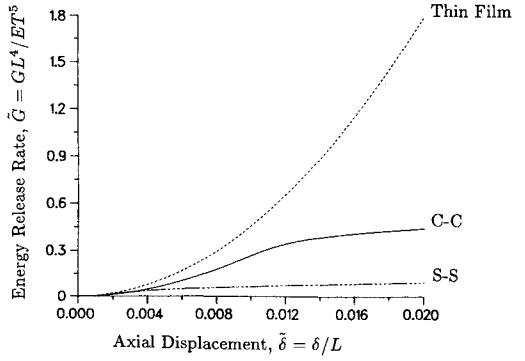

Fig. 6 Strain energy release rate vs axial displacement curves for a delaminated beam/plate with $H/T = 1/15$, $l/L = 1/2$. The cases of both clamped-clamped (C-C) and simply supported (S-S) ends are shown. The dashed curve represents the thin film approximation.

simply-supported case giving much smaller values. The significant observation is, however, that the $G - \delta$ curves eventually level out. This means that growth, if it should occur, would take place in the initial postbuckling phase. The thin film approximation predicts a higher value of the energy release rate and, most important, gives a curve of continuously increasing slope. This would predict that growth would almost certainly occur if the applied displacement is increased sufficiently. Test results that will be described later do not support this notion.

To study the effect of the location of the delamination through the thickness, load vs axial displacement curves for a delaminated beam/plate with clamped-clamped ends are shown in Fig. 7 for the cases of $H/T = 1/15$ and $1/30$. The load is normalized with respect to the buckling load for the undelaminated beam/plate P_{glo}. A constant delamination length $\ell/L = 1/2$ is assumed. The load for the case of the delamination closer to the surface ($H/T = 1/30$) is somewhat higher. Notice that the thin film model (dashed curve) gives almost identical $P - \delta$ curves for the two cases. In a similar fashion, the strain energy for the case of the delamination closer to the surface ($H/T = 1/30$) is somewhat higher (Fig. 8). On the contrary, the energy release rate for the case of $H/T = 1/30$ is substantially lower (Fig. 9). Thus, growth is less likely to occur in delaminations closer to the surface. This same effect is also predicted by the thin film approximation.

As was said previously, the thin film approximation neglects any bending deformation in the base plate and assumes the slope at the interface section equal to $\theta = 0$. An indication of the amount of the induced bending is obtained by plotting the angle θ with the applied axial displacement (Fig. 10). The effects of the location of the delamination through the thickness and the end fixity conditions are also illustrated. A constant delamination length $\ell/L = 1/2$ is assumed. The angle θ is increasing at a much faster rate after the point at which the load is leveling out. Somewhat lower values of θ occur for a delamination closer to the outer surface.

As was mentioned in the beginning, this paper is concerned with the case of local buckling only, i.e., when buckling is initiated by the local buckling of the upper delaminated layer. Therefore, it was natural to compare with the predictions of the thin film model, which is also focusing on the characteristics of this mode of instability. Other investigators[1,2,4] have considered more refined approaches, focusing on other important issues. (For example, Ref. 4 focuses on the bending-stretching effects.)

Specifically, Refs. 2 and 4 do consider the effect of including the induced bending in the base and lower parts, but they are based on representing the deflections of the upper part from the solution of the corresponding differential equation of the linearized theory of elasticity. To show the effect of the nonlinearities, a comparison was made with the predictions of Ref. 2. Figure 11a shows the load carried by the upper delaminated layer P_u vs applied displacement for the case $H/T = 2/15$, and it is seen that a higher value of the load is predicted if the nonlinearities are included. The relevant calculations also showed that neglecting the nonlinearities would give much lower values of the strain for the delaminated layer at large applied displacements.

Fig. 11b shows the energy release rate vs applied displacement, and it is seen that likewise higher values for the energy release rate are predicted due to the effect of nonlinearities. The trends are similar with the slope of the curves diminishing in both cases. At higher H/T ratios it also was found that including the large deformation effects results in the slope of the energy release rate curves decreasing at a much higher rate with applied deformation.

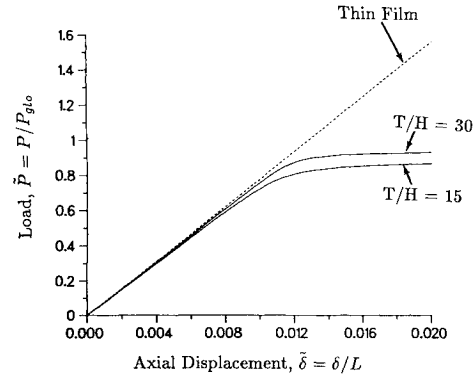

Fig. 7 Load vs axial displacement curves for a delaminated beam/plate with clamped-clamped ends illustrating the effect of the location of the delamination through the thickness. A constant delamination length $l/L = 1/2$ is assumed. Notice that the thin film model (dashed curve) gives almost identical $P - \delta$ curves for the two cases.

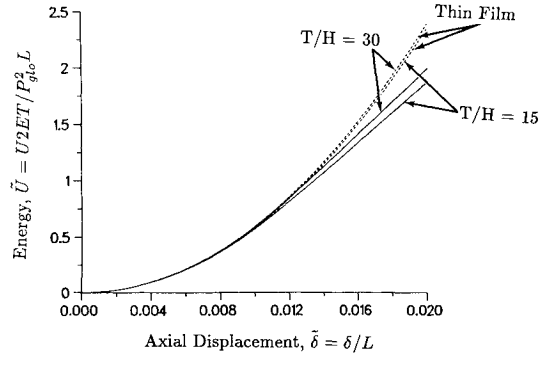

Fig. 8 Energy vs axial displacement curves for a delaminated beam/plate with clamped-clamped ends, illustrating the effect of the location of the delamination through the thickness. A constant delamination length $l/L = 1/2$ is assumed. The dashed curves represent the thin film approximation.

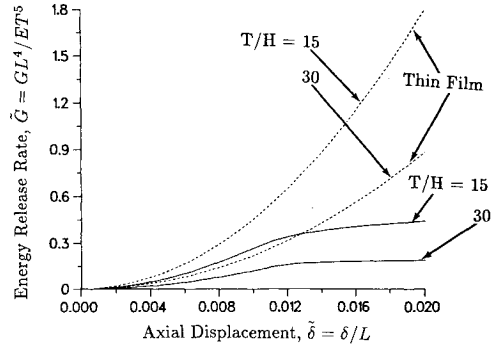

Fig. 9 Energy release rate vs axial displacement curves for a delaminated beam/plate with clamped-clamped ends, illustrating the effect of the location of the delamination through the thickness. A constant delamination length $l/L = 1/2$ is assumed. The dashed curves represent the thin film approximation.

Test Results

Tests were conducted on delaminated specimens. The specimens were made of 15 plies of unidirectional (0 deg angle ply) prepreg kevlar 49 of the following specifications: commercial type SP-328, nominal thickness per ply 0.20 mm (0.008 in.), nominal stiffness $E = E_1 = 75.8$ GN/m^2 (11×10^6 psi), $E_2 = 5.5$ GN/m^2 (0.8×10^6 psi), $G_{12} = 2.1$ GN/m^2 (0.3×10^6 psi), Poisson's ratio $\nu_{12} = 0.34$. A delamination of length $\ell = 50.8$ mm (2 in.) was introduced by a 0.025 mm (0.001 in.) thick Teflon strip placed in the middle of the length between first and second ply and through the width. The length between the grips for the specimens was $L = 101.6$ mm (4 in.). A width of 12.7 mm (0.5 in.) was used to keep the load level small and

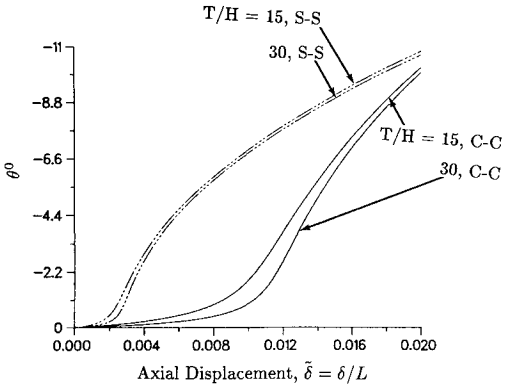

Fig. 10 Angle θ at the interface section vs axial displacement curves for a delaminated beam/plate illustrating the effect of the location of the delamination through the thickness and the end fixity conditions (clamped-clamped vs simply supported). A constant delamination length $l/L = 1/2$ is assumed. Notice that the thin film approximation assumes a slope of $\theta = 0$ during postbuckling.

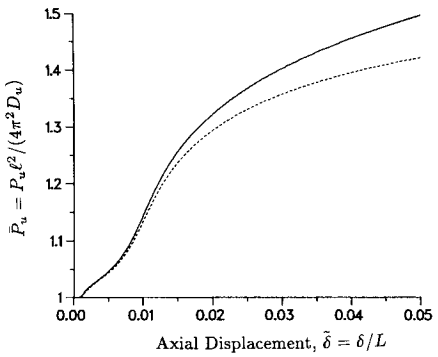

Fig. 11a Load carried by the upper delaminated layer vs displacement for a delaminated beam/plate with clamped-clamped ends and $H/T = 2/15$, $l/L = 1/2$, as predicted from the present formulation (solid line) and from Ref. 2 (dashed line). The load is normalized with respect to the Euler buckling load of the thin delaminated layer.

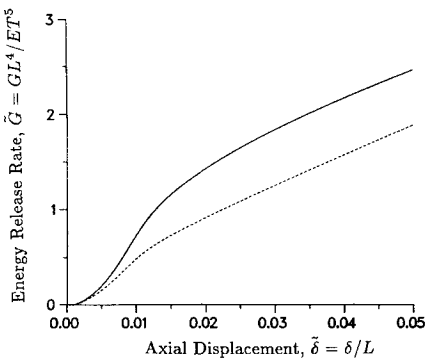

Fig. 11b Energy release rate vs axial displacement curves for the case of Fig. 11a, as predicted from the present formulation (solid line) and from Ref. 2 (dashed line).

prevent any possible bending of the grips. Since the curing process affects the final dimensions, the exact thickness for each specimen was measured (with a micrometer) after curing. The specimens were found to have a length over thickness ratio $L/T \simeq 24$. In addition, the exact modulus also was measured after curing, from a simple tension test on strain gauged coupons, and it was found to be $E = 68.2$ GN/m^2 (9.9×10^6 psi). The tests were conducted in a 20-kip MTS servohydraulic machine. They were carried out on stroke control with a rate

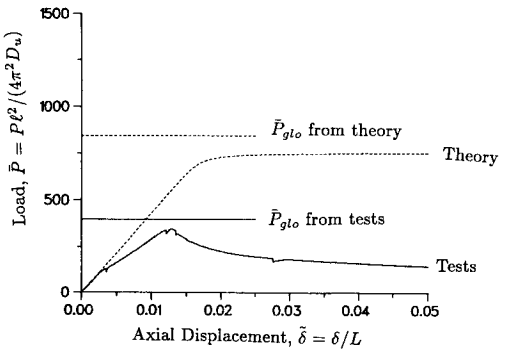

Fig. 12 Load vs axial displacement curve as obtained from compression tests on clamped-clamped delaminated specimens with $T = 4.19$ mm (0.165 in.), $L = 101.6$ mm (4 in.), $H/T = 1/15$, $l/L = 1/2$ (solid line) and as predicted from the large deformation analysis (dashed line). The buckling load levels for the undelaminated specimen P_{glo} as obtained from tests, and the analysis also are shown.

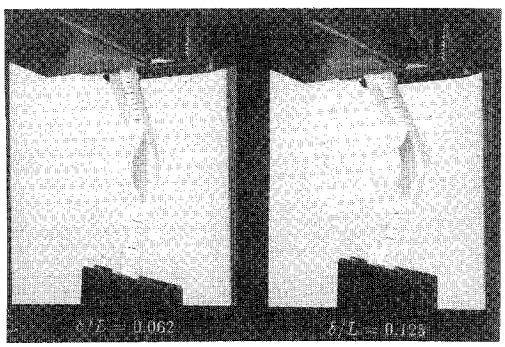

Fig. 13 The shape of the postbuckled configuration for the test specimens at the point of applied displacement a) $\delta/L = 0.062$ and b) $\delta/L = 0.125$. No growth of the delamination was observed.

of about 0.8 mm per minute. The specimen was clamped at the upper grip and a special fixture at the lower grip. The latter one was designed so that the specimen slides into it, and therefore no bending is introduced by tightening the end. To be able to compare with any theoretical model, the compliance of the testing machine also is needed. It was measured from a simple compression test (without a specimen) and was found to be 0.685×10^{-4} mm/N (0.12×10^{-4} in./lb).

Four specimens were tested, and the response curves were almost identical. A load vs axial displacement curve from the tests is shown in Fig. 12, together with the curve that is predicted from the analysis (large displacement model). The specimen for these curves had a thickness of $T = 4.19$ mm (0.165 in.). In deriving the theoretical curve, the compliance of the testing machine was added. Furthermore, specimens without delaminations were tested in order to obtain the buckling load for the undelaminated case (global buckling load) P_{glo}. This load level is also shown in Fig. 12, together with the theoretical value.

There are two things worth mentioning in the context of this work. First, there is qualitative similarity between the theoretical and experimental curves with the load peaking out at a point below the global buckling point. Although the displacement levels are basically comparable, the experimental load level is less than the theoretical one by about a factor of two. This is true for the undelaminated specimens as well and is not surprising in experimenting with buckling[6] because of the inherent difficulties in fulfilling accurately the theoretical assumptions. Specifically, various kinds of imperfections, such as some unavoidable initial curvature of the specimens, possible eccentricity in application of the load, or nonhomogeneity of the material results in lower load levels. To mention an-

other influence, lower load results due to the effect of transverse shearing forces[1] as well. Furthermore, all the tests showed a slowly dropping load after peak load. This load drop could be partly due to local cracking of fibers or matrix. At further stages of applied deformation, this was verified by the sound of the cracking fibers.

Second and more important, no growth was ever observed in these tests. Figure 13 shows the shape of the postbuckled configuration for the test specimen of Fig. 12, at the point of applied displacement $\delta/L = 0.062$ and 0.125 (which are far beyond the peak load). No growth is seen. The experiment was continued up to the displacement level of $\delta/L = 0.250$, and even at that point no growth was seen; instead, fiber cracking on the lower part took place. As predicted by the present formulation, this behavior is in agreement with the leveling out of the energy release rate curves in Fig. 6. (which means that growth, if it had not taken place initially, is not expected to occur with continuing applied displacement).

Conclusions

A one-dimensional model was developed for studying the postbuckling behavior of composites with thin film delaminations. The analysis includes large deformation effects for the delaminated layer, and the results are compared with a relevant simplified model (thin film model). In particular, the results of this work can be summarized as follows:

1) Bending deformation is necessarily induced in both the lower part and the base plate. Therefore, although instability is initiated by the local buckling of the delaminated film, transverse deflections cannot be limited to that postbuckled shape of the film only.

2) A reduced stiffness (as compared to the thin film analysis that neglects the effects of large displacements) is predicted, with the $P - \delta$ curve leveling out.

3) The end fixity (clamped-clamped vs simply supported) conditions significantly affect the postbuckling behavior.

4) The energy release rate vs axial displacement ($G - \delta$) curves level out. This means that delamination growth, unless it occurs in the initial postbuckling phase, is not expected to occur with continuing deformation.

5) Tests were conducted on delaminated specimens of unidirectional prepreg kevlar 49. There is qualitative similarity of the load-displacement curves from tests with the curves of the theory with the load peaking out and the displacement levels being comparable. The experimental load levels for both the delaminated and the undelaminated specimens are uniformly lower than the theoretical ones by a factor of about two (which is not unusual in experimenting with buckling), due to initial imperfections. More important, no growth of the delamination was ever observed in these tests, which agrees with the leveling out of the energy release rate curves, as predicted by the present formulation.

References

[1]Kardomateas, G. A. and Schmueser, D. W., "Buckling and Postbuckling of Delaminated Composites Under Compressive Loads Including Transverse Shear Effects," *AIAA Journal,* Vol. 26, March 1988, pp. 337–343.

[2]Yin, W.-L., Sallam, S. N., and Simitses, G. J., "Ultimate Axial Load Capacity of a Delaminated Beam-Plate," *AIAA Journal,* Vol. 24, 1986, pp. 123–128.

[3]Chai, H., Babcock, C. D., and Knauss, W. G., "One Dimensional Modelling of Failure in Laminated Plates by Delamination Buckling," *International Journal of Solids and Structures,* Vol. 17, 1981, pp. 1069–1083.

[4]Yin, W.-L., *Cylindrical Buckling of Laminated and Delaminated Plates, Proceedings of the 27th SDM AIAA/ASME/ASCE/AHS Conference,* AIAA, New York, May 1986, pp. 165–179.

[5]Britvek, S. J. *The Stability of Elastic Systems,* Pergamon, New York, 1973.

[6]Timoshenko, S. P. and Gere, J. M., *Theory of Elastic Stability,* McGraw-Hill, New York, 1961, pp. 1–3 and 132–135.

[7]Budiansky, B. and Rice, J. R., "Conservation Laws and Energy-Release Rates," *Journal of Applied Mechanics,* Vol. 40, 1973, pp. 201–203.

[8]Yin, W.-L. and Wang, J. T. S., "The Energy-Release Rate in the Growth of a One-Dimensional Delamination," *Journal of Applied Mechanics,* Vol. 51, 1984, pp. 939–941.